SF2A 2008
C. Charbonnel, F. Combes and R. Samadi (eds)

MULTI-TECHNIQUE OBSERVATIONS AND MODELING OF PROTOPLANETARY DISKS

Pinte, C.[1], Ménard, F.[2], Duchêne, G.[2] and Augereau, J.C.[2]

Abstract. Most of the studies on circumstellar disks are based on models that put an emphasis on fitting either SEDs or scattered light images or molecular emission maps. In this contribution, we present a more general approach which aims at interpreting the increasing amount of observational data in the framework of a single model, in order to obtain a more global picture and to better characterize both the dust population and the gas disk properties. The main objective of this general method is to couple the constraints from the gas- and dust-oriented studies to shed light on aspects of the disk structure that are cannot otherwise be studied in a coherent manner.

1 Numerical modeling

1.1 Radiative transfer code

Synthetic images, spectral energy distributions and molecular emission maps are computed using MCFOST, a 3D continuum radiative transfer code based on the Monte-Carlo method (Pinte et al. 2006). It includes multiple scattering with a complete treatment of polarization, dust heating and continuum thermal re-emission. Dust properties may vary with location within the disk, allowing us to model vertical dust settling (e.g. IM Lupi) or increase of ice mantles from the inner, hot regions to the outer, cold edge of the disk (e.g. IRAS 04158+2805). NLTE radiative transfer in molecular lines has recently been implemented in MCFOST. Calculations are performed using a long-characteristic Monte Carlo method similar to the one presented in Hogerheijde & van der Tak (2000).

1.2 Model definition

We assume a simple disk geometry, with a gaussian vertical profile: $\rho(r,z) = \rho_0(r)\,\exp(-z^2/2\,h(r)^2)$ valid for a vertically isothermal, hydrostatic, non self-gravitating disk. We use power-law distributions for the surface density $\Sigma(r) = \Sigma_0\,(r/r_0)^p$ and the scale height $h(r) = h_0\,(r/r_0)^\beta$, where r is the radial coordinate in the equatorial plane, h_0 the scale height at the radius $r_0 = 100\,\mathrm{AU}$. We consider homogeneous spherical grains and calculate optical properties with the Mie theory. The grain sizes are distributed according to the power-law $\mathrm{d}n(a) \propto a^{-3.5}\,\mathrm{d}a$, with $a_{\min}$ and $a_{\max}$ the minimum and maximum sizes of grains.

2 IM Lupi

IM Lupi (Schwartz 82) is an M0 T Tauri star, with a modest emission-line activity but surrounded by a large amount of dust. We have performed a simultaneous modeling of the various observations (SED, infrared spectroscopy, multi-wavelength scattered light images and millimeter visibilities) and analyzed a grid of models over a large fraction of the parameter space via Bayesian inference. The best model can reproduce all of the observations of the disk (Fig 1). Our analysis illustrates the importance of combining a wide range of observations in order to fully constrain the disk model, with each observation providing a strong constraint

[1] School of Physics, University of Exeter, Stocker Road, Exeter EX4 4QL, United Kingdom
[2] Laboratoire d'Astrophysique de Grenoble, CNRS/UJF UMR 5571, 414 rue de la Piscine, B.P. 53, F-38041 Grenoble Cedex 9, France

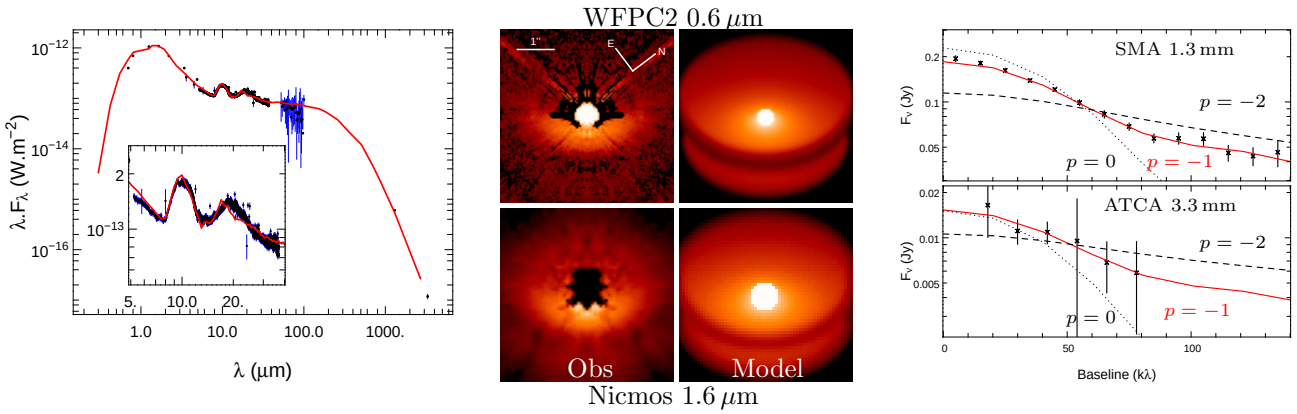

Fig. 1. Comparison of the best model with observations (Pinte et al. 2008). *Left:* SED and *Spitzer/IRS* spectroscopy. *Center: HST/WFPC2 and Nicmos* scattered light images. *Right:* millimeter visibilities. Only the model with a surface density $p = -1$ can reproduce the visibilities.

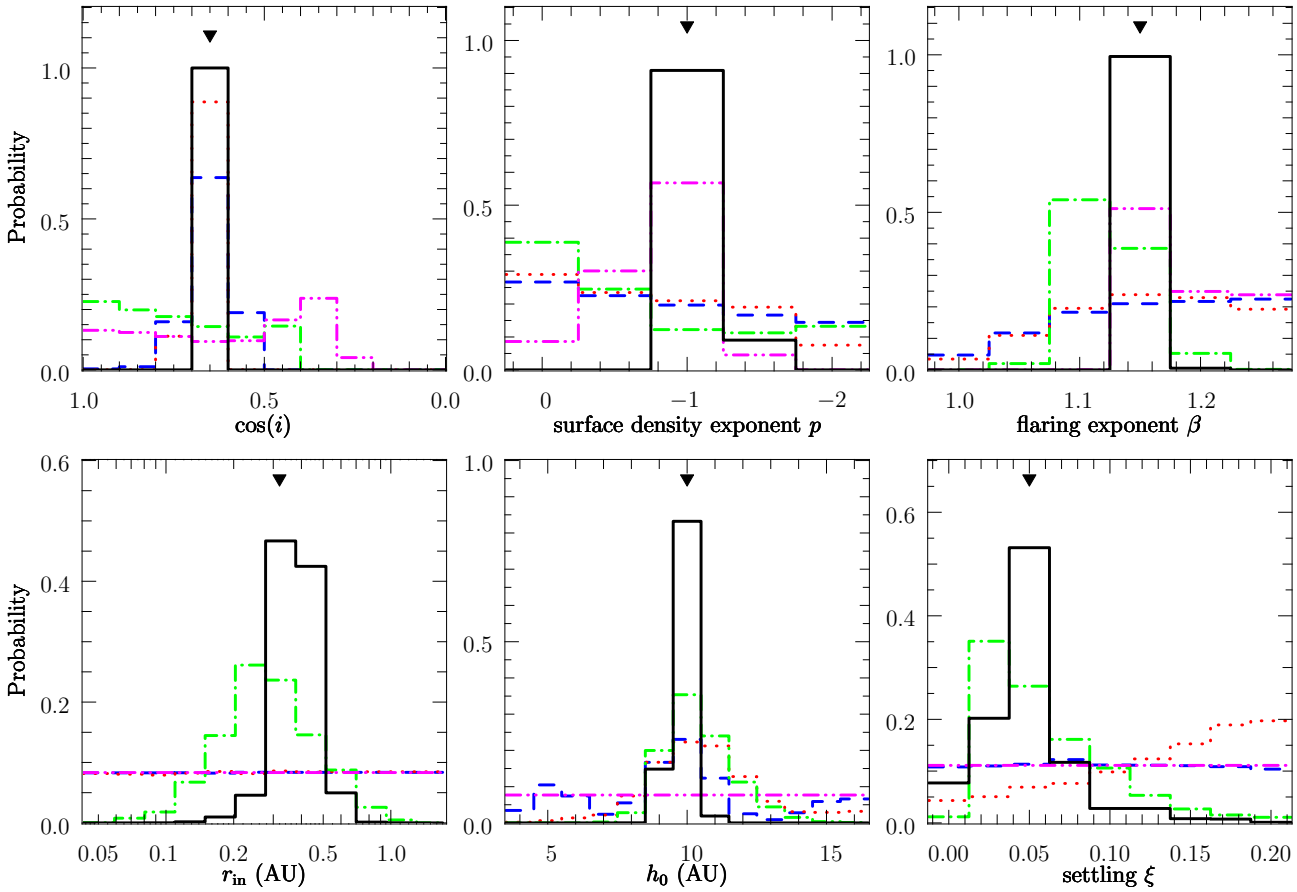

Fig. 2. Bayesian probabilities of the various parameters for the scattered light images at 0.6 μm (dashed blue) and 1.6 μm (dotted red), the SED (dot-dash green), the millimeter visibilities (dot-dot-dash pink) and for the images, SED and mm visibilities simultaneously (full black line). The triangles represent the parameters of the best model (Pinte et al. 2008).

only on some aspects of the disk structure and dust content (Fig 2). Quantitative evidence of dust evolution in the disk is obtained: grain growth up to millimeter-sized particles, vertical stratification of dust grains with micrometric grains close to the disk surface and larger grains which have settled towards the disk midplane, and possibly the formation of fluffy aggregates and/or ice mantles around grains (Pinte et al. 2008).

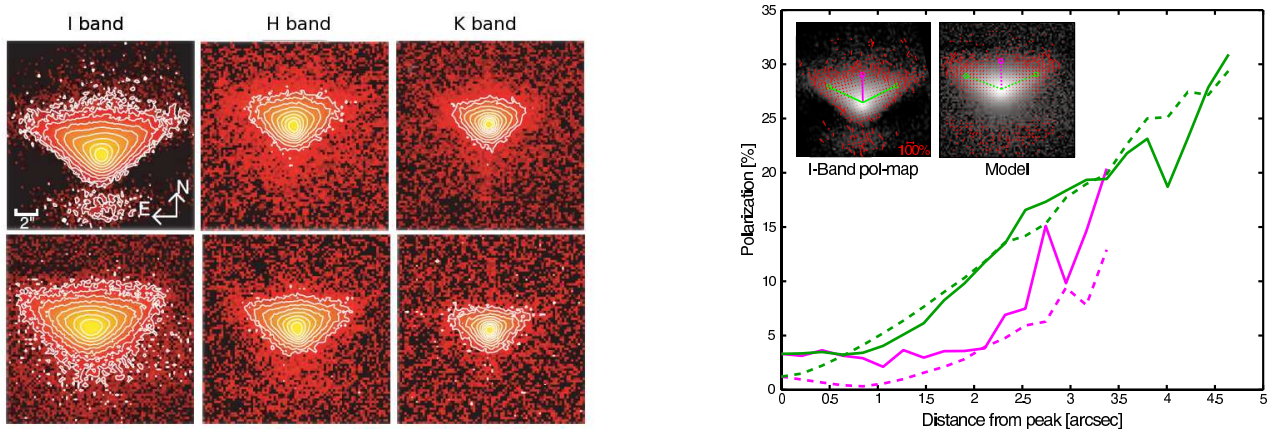

Fig. 3. *Left panel:* comparison of observed (top) and synthetic (bottom) images in I band (left), H band (center), and K band (right) of IRAS 04158+2805. Contour levels are $I = I_{\max} 2^{-n}$ with $n = 1 \ldots 8$. *Right panel:* comparison of the polarization level as a function of the position in the observed (solid) and modeled (dashed) nebula. Polarization (red vectors in insets) is compared along the ridge (green) and symetry axis (pink) of the nebula (Glauser et al. 2008).

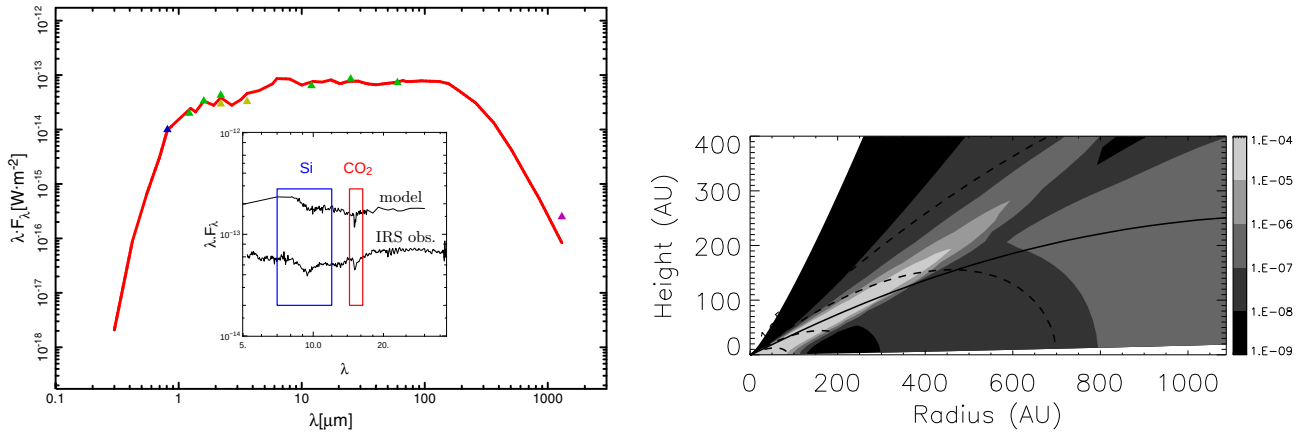

Fig. 4. *Left panel:* comparison of the observed (triangles) and modeled (red line) SEDs (Glauser et al. 2008). The SED, reminiscent of a class I is reproduced by a close to edge-on disk around a class II source. The IRS spectrum (inset) presents silicate and CO_2 absorption features (flux level is arbitrarily shifted), also seen in the model (CO_2 was added in disk regions where $T_{\rm dust} < 50\,{\rm K}$). *Right panel:* Calculated CO abundance as a function of the position within the disk.

3 IRAS 04158+2805

3.1 Modeling of the dust phase

IRAS 04158+2805 is an M5 star, near the substellar boundary. It presents evidence of circumstellar dust up to a large radius ($\approx 1\,100\,{\rm AU}$). We interpret optical and near-IR images, (VLT-FORS1, CFHT-IR), I band polarization map (VLT-FORS1), mid-infrared spectrum (SPITZER-IRS) and the SED in terms of a central star surrounded by an axisymmetric circumstellar disk, but without an envelope, to test the validity of this simple geometry. All the observations can be succefully reproduced with such a disk model observed at a grazing incidence. This allows us to establish strong constraints on the geometry of the disk and on its dust content (Fig. 3 and 4, Glauser et al. 2008).

3.2 Modeling of the gas phase

The density, temperature profiles and UV flux density derived from dust modeling are used to calculate the CO abundance throughout the disk (Fig. 4, right panel), by considering that CO molecules freeze-out onto the dust

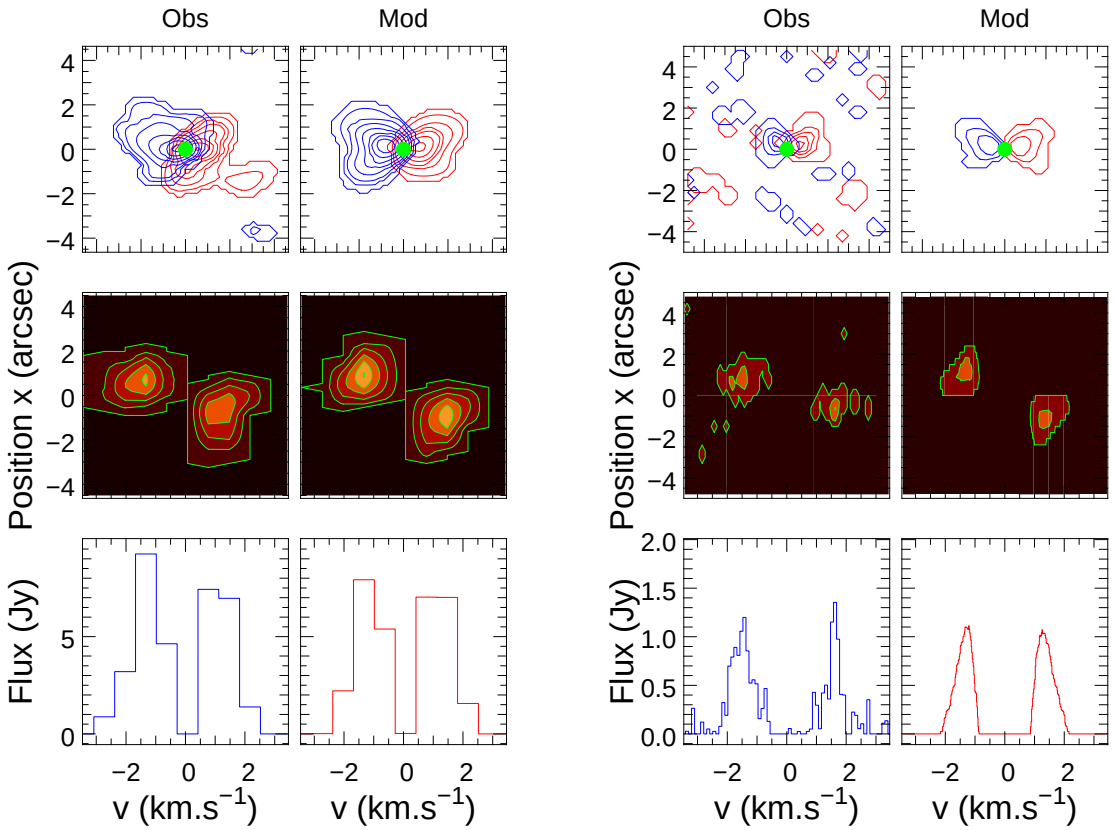

Fig. 5. Comparison of the observed and synthetic emission maps (top), position-velocity diagrams (middle) and integrated spectra (bottom). Left panel is for the J=3-2 SMA observations and right panel is for the J=2-1 IRAM/PdB observations.

grains in the midplane and are photo-dissociated by the FUV in the upper layers (Ceccarelli & Dominik 2005). From these abundances, the level populations of the CO molecules and corresponding emission maps are calculated with MCFOST (Fig. 5, Pinte et al, in prep.). Both the dust and gas observations of the disk can be reproduced consistently within the framework of this single model. The modeling allows us to constrain further the thermal and cinematic structures at large scale in the disk and additional information on the mass of the central object (in the range 0.3-0.5 $M_\odot$) and on the turbulence velocity ($\approx 0.3\,\mathrm{km.s^{-1}}$) is obtained.

4 Conclusion

The interest of the approach we present here is to combine coherently the disk density and temperature structure calculated using the dust disk geometry, as provided by continuum tracers to the different pieces of information provided by gas line tracers. The bulk of the disk mass is in the gas phase, but because most of the heating is provided by absorption of energy by dust, it is important (although difficult) to combine both approaches to improve curent modeling efforts of complex data sets. Such a global approach is needed to fully exploit present observational data sets and to prepare observations with future instruments like Herschel and ALMA.

References

Ceccarelli, C. & Dominik, C. 2005, A&A 440, 583–593
Glauser, A. M., Ménard, F., Pinte, C., Duchêne, G., Güdel, M., Monin, J.-L., & Padgett, D. L. 2008, A&A 485, 531–540
Hogerheijde,M. R. , & van der Tak, F. F. S. 2000, A&A 362, 697–710
Pinte, C. , Ménard, F. , Duchêne,G. , & Bastien, P. 2006, A&A 459, 797–804
Pinte, C. , Padgett, D.L. , Ménard, F. et al. 2008, A&A accepted, astro-ph/0808.0619